Atmos. Meas. Tech., 9, 5853–5867, 2016
www.atmos-meas-tech.net/9/5853/2016/
doi:10.5194/amt-9-5853-2016

Atmospheric Measurement Techniques
Open Access
EGU

A strategy for the measurement of CO_2 distribution in the stratosphere

Massimo Carlotti[1], **Bianca Maria Dinelli**[2], **Giada Innocenti**[1], **and Luca Palchetti**[3]

[1]Dipartimento di Chimica Industriale "Toso Montanari", Università di Bologna, Bologna, Italy
[2]Istituto di Scienze dell'Atmosfera e del Clima, ISAC-CNR, Bologna, Italy
[3]Istituto Nazionale di Ottica, INO-CNR, Sesto Fiorentino (FI), Italy

Correspondence to: Massimo Carlotti (massimo.carlotti@unibo.it)

Received: 1 July 2016 – Published in Atmos. Meas. Tech. Discuss.: 5 August 2016
Revised: 7 November 2016 – Accepted: 15 November 2016 – Published: 8 December 2016

Abstract. In this study we introduce a new strategy for the measurement of CO_2 distribution in the stratosphere. The proposed experiment is based on an orbiting limb sounder that measures the atmospheric emission within both the thermal infrared (TIR) and far-infrared (FIR) regions. The idea is to exploit the contribution of the pure rotational transitions of molecular oxygen in the FIR to determine the atmospheric fields of temperature and pressure that are necessary to retrieve the distribution of CO_2 from its rovibrational transitions in the TIR. The instrument envisaged to test the new strategy is a Fourier transform spectrometer with two output ports hosting a FIR detector devoted to measuring the O_2 transitions and a TIR detector devoted to measure the CO_2 transitions. Instrumental and observational parameters of the proposed experiment have been defined by exploiting the heritage of both previous studies and operational limb sounders. The performance of the experiment has been assessed with two-dimensional (2-D) retrievals on simulated observations along a full orbit. For this purpose, optimal spectral intervals have been defined using a validated selection algorithm. Both precision and spatial resolution of the obtained CO_2 distributions have been taken into account in the results–evaluation process. We show that the O_2 spectral features significantly contribute to the performance of CO_2 retrievals and that the proposed experiment can determine 2-D distributions of the CO_2 volume mixing ratio with precisions of the order of 1 ppmv in the 10–50 km altitude range. The error budget, estimated for the test case of an ideal instrument and neglecting the spectroscopic errors, indicates that, in the 10–50 km altitude range, the total error of the CO_2 fields is set by the random component. This is also the case at higher altitudes, provided the retrieval system is able to model the non-local thermal equilibrium conditions of the atmosphere. The best performance is obtained at altitudes between 20 and 50 km, where the vertical resolution ranges from 3 to 5 km, and the horizontal resolution is of the order of 300–350 km depending on latitude.

1 Introduction

The role of CO_2 in the radiative budget of the biosphere is well established as well as the consequences of its growth on the Earth's climate. The knowledge of CO_2 abundance and distribution is then essential to monitor the evolution of global warming and to drive the appropriate political choices. The remote sensing techniques with instruments on board orbiting platforms have been demonstrated to represent a powerful strategy for monitoring the atmospheric state. In the case of CO_2, it can be easily detected in the infrared spectral region (both near infrared, NIR, and thermal infrared, TIR), where the spectral features generated by its rovibrational transitions are clearly visible. A number of space missions have been designed to measure CO_2 from space (Chédin et al., 2003; Crevoisier et al., 2004, 2009; Kulawik et al., 2010; Buchwitz et al., 2005; Kuze et al., 2009; Boesch et al., 2011); most of them aim to measure tropospheric abundances and use the nadir observation geometry that is suitable for column measurements. Limb observations are more appropriate than nadir observations for discriminating the atmospheric behaviour at different altitudes. Actually, limb-scanning spectrometers have been widely used to obtain the distribution of

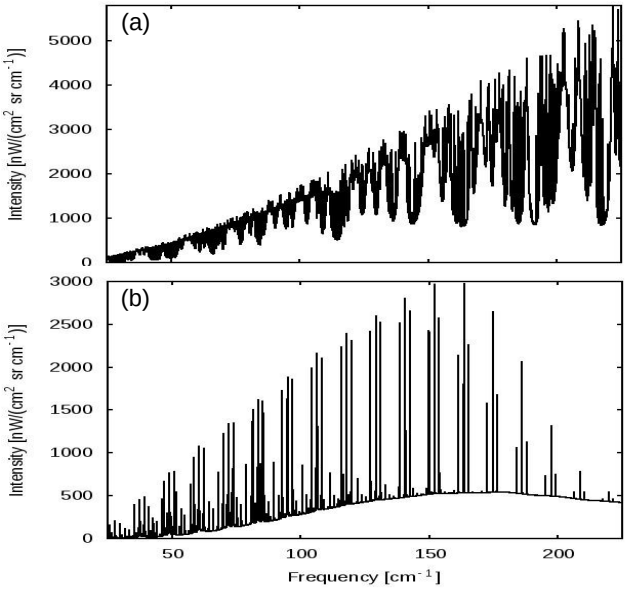

Figure 1. (a) Far-infrared atmospheric spectrum simulated at 20 km tangent altitude, **(b)** same as upper panel but only O_2 is included in the simulation.

physical and chemical parameters in the stratosphere and upper troposphere and to monitor their evolution over the years. Some limb experiments, such as the Michelson Interferometer for Passive Atmospheric Sounding, MIPAS (Fischer et al., 2008) and the High Resolution Dynamics Limb Sounder, HIRDLS (Gille et al., 2008), exploit the CO_2 rovibrational transitions to determine pressure (P) and temperature (T) fields that, besides their intrinsic importance, are necessary in the data analysis to retrieve any target molecule from its spectral features. In these experiments, the P, T retrieval process is based on the assumption that the CO_2 distribution is known. This assumption prevents the CO_2 spectral features from being used for the retrieval of its own atmospheric distributions. To date, only the Atmospheric Chemistry Experiment (ACE – Bernath et al., 2005) has provided daytime measurements of the CO_2 altitude distribution between 5 and 25 km and in the mesosphere (Foucher et al., 2011; Emmert et al., 2012; Sioris et al., 2014). In these measurements, the accuracy of a single profile is of the order of 10 ppmv (Foucher et al., 2009). The big challenge for ACE (which performs occultation measurements in the TIR region) was to retrieve P and T (and pointing information at low altitudes) from spectral signals that are generated by different sources from the CO_2 transitions. A thorough discussion about the strategies that space experiments have used to measure CO_2 in the atmosphere can be found in Foucher et al. (2011).

In this study we propose a new strategy for the measurement of CO_2 atmospheric distribution using a passive orbiting limb sounder. The starting idea is to exploit the pure rotational transitions of molecular oxygen (O_2) in the far-infrared (FIR) region for the retrieval of the P and T fields, which are necessary to retrieve the CO_2 distribution from its transitions in the TIR region. This strategy is expected to uncouple the strong correlation between T and CO_2 volume mixing ratio (VMR), which is intrinsic to the analysis of the TIR spectral features of CO_2. As the O_2 rotational transitions originate from a magnetic dipole moment, their line strengths are very low; nevertheless, due to both the huge abundance of O_2 and the long optical path of limb observation geometries, they are among the most prominent features of the atmospheric spectrum below 200 cm^{-1} (Carli and Carlotti, 1992). This is illustrated in Fig. 1, where the upper panel shows the simulated FIR atmospheric emission at 20 km tangent altitude (as observed by the spectrometer described in Sect. 2) and the lower panel shows the FIR emission when only O_2 is included in the simulation. The compressed scale of Fig. 1 prevents the identification of O_2 lines in the upper panel. However, the comparison of the two panels shows that, below 170 cm^{-1}, the intensity of the O_2 lines matches the maximum emission of the atmospheric spectrum. On the basis of these considerations we suggest using an instrument capable of measuring simultaneously the atmospheric FIR O_2 lines and the TIR CO_2 lines to determine the VMR of CO_2 stratospheric fields with the target precision of 1 ppmv. For this purpose, we propose to exploit a Fourier transform (FT) spectrometer with two output ports hosting a FIR detector to measure O_2 pure rotational transitions and a TIR detector to measure CO_2 rovibrational transitions in the 700–900 cm^{-1} region (roughly corresponding to MIPAS band A). The preliminary question to answer in our study is about the real contribution that the O_2 transitions can provide to the precision of the retrieved CO_2 VMRs. Actually, at stratospheric temperatures, the Planck function and its sensitivity to T are much lower in the FIR region than in the TIR region where CO_2 features will have to be analysed (the steep growth of the Planck function can be appreciated in the upper panel of Fig. 1). This suggests that the precision of the T values retrieved only from FIR transitions could not be sufficient to satisfactorily determine the CO_2 distribution from its TIR transitions. Moreover, a crucial step is to define experimental and retrieval conditions that are suitable to determine CO_2 VMRs with the required precision in the stratosphere and upper troposphere (extending as low as possible the altitude range at which these precisions are achievable).

This academic study is directed to assess the intrinsic capability of the proposed approach irrespective of some technological aspects that need to be evaluated when an operational experiment is considered.

In Sect. 2 of this paper we define the instrumental and observational parameters of the proposed experiment (which we will call OXYCO2), and we discuss the selection of the optimal spectral intervals to be used for the analysis on simulated observations. Section 3 is devoted to describe the strategy adopted for the retrievals on simulated observations while the results of the retrieval tests are shown and discussed

in Sect. 4. Finally, in Sect. 5 we draw the conclusions of our study.

2 Operational parameters

2.1 Instrumental and observational parameters

The instrumental and observational parameters for OXYCO2 have been defined by exploiting the heritage of previous experiments, whether implemented (MIPAS and SAFIRE, Spectroscopy of the Atmosphere by Far-Infrared Emission, Bianchini et al., 2004) or designed for future missions with the support of documented studies (PIRAMHYD, Passive Infrared Atmospheric Measurements of Hydroxyl, 1998 and IRLS, Infrared Limb Sounder, of the PREMIER, Process Exploration through Measurements of Infrared and millimetre-wave Emitted Radiation, experiment) (Kraft et al., 2011). The OXYCO2 experiment is based on a limb-scanning FT orbiting spectrometer with two output ports hosting a FIR detector (to measure the O_2 emission) and a TIR detector (to measure the CO_2 emission). The SAFIRE spectral resolution of $0.004\,cm^{-1}$ (FT) has been adopted for OXYCO2. This relatively high value is meant to avoid, as much as possible, systematic errors due to transitions of interfering species (see Sect. 4.4) and to enhance the sensitivity of the measurements. A similar spectral resolution, which mainly helps at high altitudes, was also suggested for the FT spectrometer in the PIRAMHYD study aimed at the measurement of the hydroxyl radical (OH) in the atmosphere.

The space platform is assumed in the same orbit of ESA/ENVISAT (Environmental Satellite), which is a sun-synchronous nearly-polar orbit at an altitude of about 700 km; the orbit period is about 101 min. The spectrometer measures the limb emission looking backwards along the orbit track (similarity to MIPAS and IRLS), which enables the use of the GMTR (geo-fit multi-target retrieval model) 2-D algorithm (Carlotti et al., 2006) in the data analysis stage (see Sect. 3). For OXYCO2, we envisage the use of one-dimensional (1-D) vertical-array detectors, which allow the measurement of a whole limb scan with a single stroke of the moving mirror (2-D array detectors were proposed for the IRLS spectrometer, which was designed to measure out of the orbit plane). A further advantage of array detectors is that the pointing accuracy translates into an angular bias which is common to all of the limb geometries and does not affect the altitude sampling step (i.e. the separation between adjacent tangent points). We assume the time of 15 s for each interferogram recording cycle. It follows that in a full orbit we can collect about 400 limb scans roughly separated by 100 km. The field of view (FOV) of about 3 km at tangent point, and the limb geometries are the same as MIPAS full resolution (FR) nominal mode (Fischer et al., 2008); tangent altitudes are separated by 3 km from 6 to 42 km and then 47, 52, 60, and 68 km. Finally, the noise equivalent spectral radiance (NESR) is assumed to be $5\,nW/(cm^2\,sr\,cm^{-1})$, consistent with the values proposed for IRLS and PIRAMHYD. The values of the spectral resolution, interferogram recording time, horizontal atmospheric sampling, and NESR are strictly interconnected. Actually, the recording time, which defines the atmospheric sampling step, is proportional to the spectral resolution and is conditioned by the detector integration time, which, in turn, affects the NESR. The NESR requirement assumed for this study is consistent with the outlined spectral measurement, which is performed with a detector-noise-limited spectrometer with an optical layout similar to the one used in SAFIRE, with an optical throughput of $0.015\,cm^2$ sr and uses 4.2 K cooled detectors. For the estimation of the NESR, the specifications of unstressed Ge : Ga detectors have been used. These detectors have already been deployed in space missions such as the ESA Infrared Space Observatory (ISO) (Lim et al., 1998) and require low temperatures that can be reached with a cryocooler system (Rogalski, 2012). The main instrumental and observational parameters of OXYCO2 are reported in Table 1.

Table 1. Instrumental and observational parameters of OXYCO2.

Orbit	sun-synchronous polar
Detectors	1-D arrays
Spectral coverage FIR	$80–180\,cm^{-1}$
Spectral coverage TIR	$685–930\,cm^{-1}$
Spectral resolution (FT)	$0.004\,cm^{-1}$
Interferogram recording time	15 s
Vertical sampling	MIPAS FR nominal mode*
Horizontal sampling	~ 100 km
NESR	$5\,nW/(cm^2\,sr\,cm^{-1})$
FOV at tangent point	3 km

* see Sect. 2.1.

2.2 Selection of optimal spectral intervals

The retrieval targets need to be defined before the selection of an optimal set of spectral intervals (MicroWindows, MWs) to be analysed in the inversion process. In our case, the spectral features of O_2 and CO_2 will have to be inverted to retrieve the atmospheric distributions of P, T, and CO_2 VMR (which is the ultimate goal). The visual inspection of observations simulated with different spectral resolutions and for different tangent altitudes shows that the main interference to the CO_2 spectral features is due to the O_3 ν_2 band rovibrational transitions. The high spectral resolution adopted for OXYCO2 reduces the O_3 interference to a level that suggests O_3 VMRs may not be included in the retrieval state vector (see discussion about this in Sect. 4.4). Nevertheless, the observations simulated in the FIR show that the interference of H_2O transitions with the O_2 spectral features cannot be avoided by acting on the spectral resolution alone. The size of the systematic errors induced by the water variability in

the inversion process is such that we decided to include H_2O VMRs in the state vector of our retrieval tests (see Sect. 4.1). For this reason, the MWs selection system was operated for the retrieval of P, T, and H_2O VMR from FIR transitions.

The MWs used for the retrievals described in this paper were selected by adapting the algorithm described in Dudhia et al. (2002) to our specific needs. For this purpose a set of error sources must be defined and quantified in order to evaluate the uncertainty associated with each spectral point. Here we have considered errors deriving from the VMR uncertainty of all of the atmospheric constituents and the error deriving from the non-local thermal equilibrium (NLTE) conditions when they are not modelled in the retrieval system. Instrumental and spectroscopic errors have been omitted in this academic study by assuming that, in the case of operational implementation, they will have to be assessed on the basis of the existing technology. The MWs selection algorithm also requires the definition of the uncertainties associated with an a priori knowledge of the state vector. The MW growing process starts from a "seed" consisting of a 2-D set of spectral points (the two dimensions being frequency and retrieval altitude) which (when inverted) carry an error budget with respect to the retrieval targets. In this process, seeds are identified by scanning the full spectral band in search of the 2-D set that carries the highest information gain. The scanning procedure is repeated in search of a new seed after each new MW has been generated. Any improvement of the errors with respect to the a priori uncertainties is quantified by the "information gain" scalar (Dudhia et al., 2002). The initial set of spectral points is left to expand in both dimensions and the information gain is calculated for the extended set (including the additional spectral point or retrieval altitude). The new set is retained in the MW if this yields an increase of information. The MW growth process continues until either the inclusion of additional elements does not yield an increase of information or the maximum MW size has been reached (we allowed for a maximum of $0.5\,\mathrm{cm}^{-1}$ which corresponds to 125 spectral points). The next MW will grow around a new seed and its information gain will be evaluated with respect to the error budget of the previously selected MW. The search for new MWs continues until the information gain obtained introducing the new MW assumes values below a fixed threshold. A consequence of this MWs selection strategy is that different combinations of MWs may be used at each altitude of the vertical retrieval grid. We remark that the MWs selection process evaluates the error budget (random and systematic) by simulating retrievals with an algorithm that operates on individual limb scans (1-D algorithm), whereas the performance of OXYCO2 will be evaluated using the 2-D GMTR algorithm (see Sects. 3, 4 and Appendix A), which operates on the whole set of limb scans of the orbit.

Within the FIR measurements, 14 MWs were generated for the retrieval of P, T, and H_2O VMR while 15 MWs were generated in the TIR for the retrieval of the CO_2 VMR. In order to limit the number of observations to be analysed, a further selection was performed among the initial set of 29 MWs using the information load (IL) analysis (Carlotti and Magnani, 2009; Carlotti et al., 2013). The basic concepts of the IL analysis are summarised in Appendix A. Both intensity and altitude coverage of the IL (with respect to the target quantities) were the criteria used to evaluate the performance of each MW. In this way, the final set of observations used in the retrieval tests reported in Sect. 4 was reduced to 15 MWs: 6 of them in the FIR and 9 in the TIR. The frequency intervals of these MWs are reported in Table 2 together with the corresponding number of spectral points and the altitude interval where the MW is used. Figure 2 shows maps of the overall IL of the selected sets of MWs along a whole orbit. The IL values in Fig. 2 (as well as all of the tests reported in this paper) have been calculated for the April 2004 atmosphere taken from the IG2 climatological database (Remedios et al., 2007); the altitude profiles of this atmosphere will be called "reference profiles". In all of the maps in this paper (Figs. 2, 4, and 8), the ground projection of the orbit track is represented by the orbital coordinate (OC), the angular polar coordinate originating at the North Pole ($\mathrm{OC} = 0$ and $360°$) and spanning the whole orbit plane (the South Pole has $\mathrm{OC} = 180°$ while the Equator has $\mathrm{OC} = 90$ and $270°$ at the descending and ascending nodes respectively). In Fig. 2 the upper-left panel shows the IL with respect to T of the 6 FIR MWs while the upper-right panel shows the IL with respect to T of the 9 TIR MWs. In the same figure the lower-left panel shows the IL with respect to the CO_2 VMR of the TIR MWs. In order to interpret these results, the lower-right panel of the Fig. 2 reports the T field of the atmospheric model used in our computations. The comparison of the maps of the IL with respect to T for the TIR and FIR MWs (note the factor of two between the scale expansions of the two upper panels of Fig. 2) highlights how much larger the information on T is in the TIR region (the IL with respect to the T of the combined set of 15 MWs is not shown because, due to the different magnitudes, the quadratic-summation combination law makes this map quite similar to the upper-right panel). Furthermore, by comparing the maps of the temperature IL of the TIR MWs to the T field we can appreciate the correlation between their minima. On the contrary, the temperature IL of the FIR MWs does not show clear correlations with the T field; this is a consequence of the T dependence of the Planck function (P_f). Actually, at a temperature of 250 K (average T in the stratosphere) $\mathrm{d}P_\mathrm{f}/\mathrm{d}T$ is of the order of $25\,\mathrm{nW/(cm^2\,sr\,cm^{-1}\,K)}$ in the FIR while the numerical value of the derivative rises to about 115 in the TIR (around $800\,\mathrm{cm}^{-1}$). Finally, in Fig. 2 we can notice that the IL with respect to T in the set of analysed observations is much higher than the IL with respect to the CO_2 VMR.

The MWs resulting from our selection are sufficient to demonstrate the measurement approach; however, we note that this selection should be revisited once improved spectroscopic error estimates are available and that inclusion of CO_2

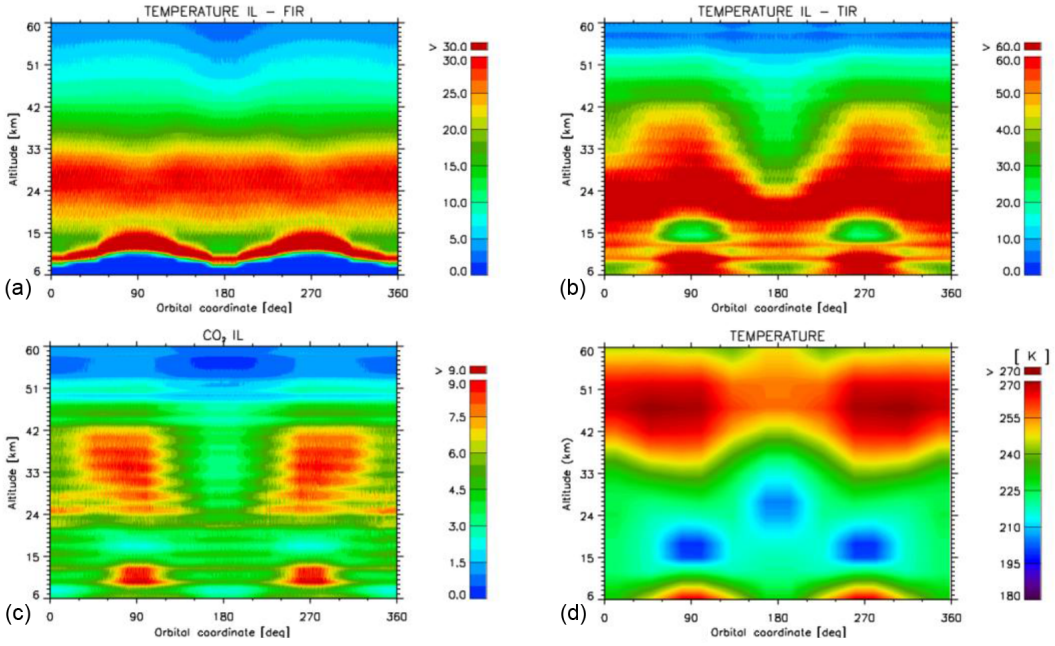

Figure 2. **(a)** IL with respect to T of the FIR MWs. **(b)**: IL with respect to T of the TIR MWs. **(c)** IL with respect to CO_2 VMR of the TIR MWs, **(d)** T field of the reference atmosphere.

Table 2. Definition of the MWs selected for the retrieval tests.

FIR			
MW number	Frequency interval (cm^{-1})	No. of points	Altitude coverage (km)
1	117.840–118.336	125	6–68
2	119.524–120.020	125	6–68
3	150.280–150.776	125	6–68
4	161.128–161.624	125	6–68
5	163.264–163.728	125	12–60
6	175.760–176.256	125	6–68
TIR			
MW number	Frequency interval (cm^{-1})	No. of points	Altitude coverage (km)
7	700.884–701.108	57	15–68
8	702.112–702.304	49	15–68
9	758.760–758.924	42	6–68
10	760.252–760.484	59	6–68
11	810.904–811.076	44	18–60
12	818.664–818.856	49	6–68
13	820.116–820.312	50	12–68
14	821.756–821.984	58	15–68
15	918.532–918.716	47	24–68

lines with less temperature dependence could potentially improve the retrieval performance.

3 Layout of the retrievals on simulated observations

Retrieval tests have been carried out on simulated observations using the 2-D GMTR analysis system (Carlotti et al., 2006), which was specifically developed for MIPAS measurements. The GMTR implements the geo-fit algorithm

(Carlotti et al., 2001a) in which the atmospheric state is allowed to vary in both the vertical and horizontal (latitudinal) dimensions. With this approach, the horizontal gradients are properly modelled by the simultaneous fit of measurements from a complete orbit. A further feature of GMTR is the multi-target retrieval (MTR) capability (Dinelli et al., 2004), which allows the simultaneous retrieval of atmospheric targets. The MTR strategy avoids the propagation of systematic errors induced by the overlapping of the spectral features of different retrieval targets when they are retrieved sequentially. We remark that when the MTR is applied to our case study (see Sect. 4.1), the information on P and T is gathered from all of the spectral features and not only from those of O_2 and/or CO_2. For the reader's convenience, Appendix A reports the basic physical and mathematical concepts behind the GMTR analysis system.

The steps of our retrievals on simulated observations are as follows.

1. Generate simulated observations with the GMTR standalone forward model. A random Gaussian noise with standard deviation equal to the instrument NESR requirement (as defined above) is added to the synthetic spectra. Reference profiles are used at this stage to provide the atmospheric model.

2. Retrieve geophysical targets from the simulated observations starting from an initial guess obtained by applying random perturbations to the reference profiles. Auxiliary data are the same as used in step 1 so that their uncertainties are not taken into account in the systematic error budget.

3. Assess the retrieval precision by comparing the retrieved values with the reference values used to generate the simulated observations. In our tests the retrieval precision includes the propagation of spectral noise and the effect of ray tracing. Actually, the 2-D ray tracing is different in the retrieval step with respect to step 1 because the perturbed values of P and T (see Sect. 4.3) cause a different behaviour of the refraction index and, therefore, slightly different paths of the lines of sight of the instrument.

4. Assess the spatial resolution of the retrieval products through the 2-D averaging kernel of the inversion process.

In simulated retrievals a crucial issue is the strategy adopted (step 2) for the generation of the initial guess of the target quantities, that is, the algorithm used for the perturbation of the reference profiles. A possible approach consists of applying a random percent perturbation (with predefined maximum amplitude) to each altitude of the reference profiles. This strategy often leads to unphysical atmospheric fields. This drawback is amplified in the 2-D approach in which the initial guess of the retrieval is a set of adjacent vertical profiles and the random perturbations at each altitude may also produce unphysical horizontal gradients of the target quantities. On the other hand, if a constant perturbation is applied to the elements of a whole profile, unphysical shapes are avoided in the vertical domain but unphysical horizontal gradients may still be present. For these reasons we have implemented the following perturbation strategy.

Once the maximum amplitude of the perturbation (B) is defined, we apply a percent perturbation (pert) to each altitude (h) of the reference profiles given by the sinusoidal function:

$$\text{pert}\,(h) = A \cdot \sin\left(2\pi\,\frac{h}{Z} + \phi\right), \tag{1}$$

where $Z = 80\,\text{km}$.

For each perturbation profile along the orbit, a random value of $A \leq B$ and a random value of ϕ between 0 and 2π is assigned.

This recipe generates a sinusoid of random amplitude (A) and phase (ϕ), which introduces a smooth variation (with altitude) of the perturbation. Since the reference (climatological) profiles are generally smooth, our perturbation strategy leads to physical shapes of the perturbed profiles. However, depending on the random value of ϕ, a perturbed profile will have altitudes that are affected by the maximum perturbation (A) and others with null perturbation. In order to assess the behaviour of our simulated retrievals with respect to a balanced altitude distribution of the perturbations, we then need to perform a number of retrieval tests which are large enough to make the perturbation almost constant with altitude when averaging the results. Figure 3 shows average altitude distributions of pert(h) (generated with Eq. 1) after a set of 20 GMTR-simulated retrievals. The five black lines of Fig. 3 correspond to perturbations calculated for $B = 1, 2, 3, 4, 5$ (values that will be used in our tests described in Sect. 4). Due to the strong variability of the tropospheric H_2O VMR, a value of B, constant at all altitudes, is not appropriate to perturb the H_2O VMR profiles. Therefore, for this target we have used $B = 30$ at the lowest altitude. This value is linearly decreased up to 15 km, at which point it becomes 10 and remains constant. The red line in Fig. 3 (measured by the upper scale) refers to the average perturbations applied to H_2O VMR profiles. In Fig. 3 we see that the average over 20 GMTR runs generates a satisfactory approximation of the constant percent values of 0.3, 0.7, 1.0, 1.3, and 1.5, which correspond to $B = 1, 2, 3, 4, 5$. The results of 20 runs have been averaged in all of the retrieval tests reported in Sect. 4.3.

4 Retrieval tests

4.1 Retrieval strategy

Preliminary tests were carried out with the "sequential retrievals" strategy previously used in the MIPAS data analysis

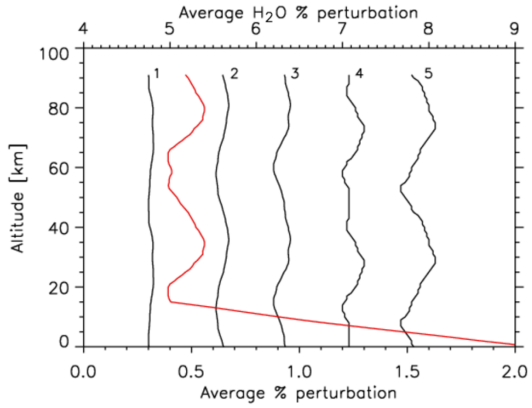

Figure 3. Average % values (over 20 GMTR runs) of pert (h) corresponding to different values of B in Eq. (1). The value of B is reported on top of each line except for the red line that refers to H_2O perturbations and is measured by the upper scale. In this case B is 30 at 0 km and linearly decreases up to 15 km where it assumes the constant value of 10.

system (Ridolfi et al., 2000). In the case of MIPAS, T and P (at tangent points) are first retrieved from the CO_2 spectral features; the VMR of atmospheric species is then derived in subsequent steps by using the previously retrieved parameters as known quantities in the forward model. In our tests P, T, and H_2O VMR were first derived from the FIR MWs, then used as known quantities in the retrieval of the CO_2 VMR from its TIR spectral features. This strategy led to CO_2 VMR precisions that did not approach the target value. We have verified that the insufficient precision of the retrieved T fields is responsible for the bad performance of the sequential strategy. The evidence is given by the precision of the CO_2 VMRs, which becomes satisfactory when, in the CO_2 analyses, we use the retrieved values of P and H_2O VMR but the reference values of T.

The retrieval strategy was then changed to fully exploit the potentiality of both the measurement strategy and the MTR functionality of the retrieval system: FIR and TIR observations were simultaneously analysed to retrieve P, T, and the VMRs of H_2O and CO_2 in a single step. As mentioned in Sect. 3, the advantage of MTR is that the information on P and T is gathered from all of the analysed spectral features (including O_2, CO_2, and H_2O). With this approach, the T dependence on the O_2 transitions reduces the correlation between T and CO_2 VMR, which is intrinsic in the analysis of CO_2 spectral features alone. Furthermore, if we look at the FIR and TIR spectra as two independent measurements sampling the Planck function in separated frequency regions, the retrieval of T is better constrained when simultaneously analysing both regions. On the other hand, the drawback of the MTR strategy is in the additional set of retrieval parameters introduced in the state vector by H_2O VMRs and atmospheric continuum parameters associated with the FIR MWs (see Sect. 4.2).

4.2 Retrieval set-up

In all of the retrieval tests performed with the above-mentioned strategy, the state vector contains the parameters describing the atmospheric field of the geophysical targets, including the atmospheric continuum (below 27 km) at the frequency of each MW. The whole set of 15 MWs (see Table 1) was used in all tests reported in the next subsection. By considering that not all of the MWs are used at each of the 17 tangent altitudes, a total of 18 904 spectral points are analysed for each limb scan; this corresponds to a total of 7 580 504 spectral points simultaneously fitted in the GMTR analysis of a full orbit. Our retrievals were carried out on a vertical grid coincident with the nominal tangent altitudes of the limb scans (see Sect. 2.1) except for the 9 km altitude, which was removed in order to improve the precision in the upper troposphere; this exclusion degrades the vertical resolution at tropospheric altitudes (see Sect. 4.3). The horizontal grid was defined with altitude profiles separated by 2 latitudinal degrees; this choice implies 180 profiles in the whole orbit and corresponds to a horizontal retrieval sampling which is about twice as wide as the measurement sampling. This set-up leads to 2880 retrieval parameters for each of the four main targets. The number of continuum parameters is 13 320 (this number does not match the product between number of retrieval altitudes, number of MWs, and number of limb scans because not the all MWs are used at all altitudes). The total number of retrieval parameters is then 24 840.

The GMTR analysis system makes use of the maximum a posteriori likelihood technique (optimal estimation). Since the initial guess of the retrieval parameters was obtained by applying "strong" perturbations (see Sect. 3), the reference profiles were used as a priori estimates of the state vector. However, large uncorrelated uncertainties (diagonal elements of the a priori variance–covariance matrix, VCM) were associated with the a priori values; they are 30 % for P, a constant error of 7 K for T, 80 % for the VMR, and 100 % for atmospheric continuum parameters. A constant term was also added to the H_2O and atmospheric continuum a priori errors to prevent strong constraints where the a priori fields assume very small values. Dedicated tests have shown that the retrieval results barely depend on the errors assigned to the a priori estimates.

4.3 Retrieval results

The IL analysis reported in Sect. 2.2 shows that the analysed observations are far more sensitive to T than to the CO_2 VMR. Therefore, in order to assess the stability of the retrieval system and its ability to sort out the information between T and CO_2 VMR in unfavourable conditions, we have also considered strongly perturbed atmospheric fields

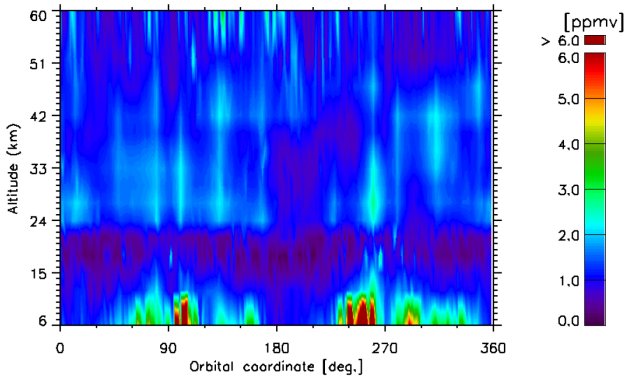

Figure 4. 2-D distribution of the averaged absolute difference between reference and retrieved CO_2 VMRs resulting from the sample test (see text).

as the initial guess for our retrieval tests (even if the perturbations might appear unrealistic). The initial guess atmospheric fields were generated by applying the perturbations generated by Eq. (1) to the reference profiles, wherein values of $B = 2, 3, 4, 5$ were used for CO_2 VMR profiles while different combinations of B values were used for the perturbation of P and T profiles. The impact of the perturbation adopted for the H_2O profiles (see Sect. 3) has been evaluated by performing retrievals keeping the perturbation of P, T, and CO_2 fixed but using different magnitudes of B for the H_2O perturbations. The difference between the retrieved CO_2 fields was negligible; therefore the perturbation reported in Fig. 3 for H_2O was kept constant in all of our tests.

In order to provide a typical example of the retrieval results, Fig. 4 shows the 2-D distribution of the average difference (absolute value) between retrieved and reference CO_2 VMRs in the case of P, T, and CO_2 initial guess profiles obtained with $B = 2$, 1, 4 respectively (this example will be called "sample test" in the following part of the paper). An overall picture representing the results shown in Fig. 4 can be given in the form of a plot (which we call the overall plot) reporting, at each altitude, the average absolute value of the differences in Fig. 4 along the whole orbit. Retrieval results in term of overall plots will be shown for the case of "weak" and "severe" perturbations of P and T profiles. The results obtained in the case of weak P, T perturbations ($B = 2$ for P and $B = 1$ for T) are reported in Fig. 5. In the four panels of this figure, the red lines show the overall plot for the CO_2 retrievals obtained by perturbing its reference profiles with values of B equal to 2 (top left), 3 (top right), 4 (bottom left), and 5 (bottom right). Figure 6 reports the same quantities of Fig. 5 but in the case of severe P, T perturbations ($B = 3$ for P and $B = 4$ for T). The red curves in Figs. 5 and 6 suggest that the retrieval is rather stable with respect to the size of the applied perturbations and that the CO_2 VMRs can be retrieved by the OXYCO2 experiment with precisions that are of the order of 1 ppmv between 10 and 50 km. To fully understand the importance of measuring FIR and TIR spectral regions together, we need to assess whether and to what extent the FIR observations are necessary and how they contribute to the precision obtained in our retrieval tests. In order to answer this question we have excluded the FIR MWs from the set of the analysed observations. Since the H_2O contribution is negligible in the TIR MWs, we have also excluded the H_2O parameters (and the atmospheric continuum of FIR MWs) from the state vector of the retrieval. In these conditions the total number of observations analysed along the full orbit is reduced to 2 663 041 while the total number of retrieval parameters is 15 660. The green lines in Figs. 5 and 6 report the overall plots of this modified retrieval set-up in the case of weak and severe P, T perturbations (H_2O profiles are unperturbed in this case). The results obtained without the FIR measurements indicate that the contribution of FIR observations to the retrieval precision is important and increases by increasing the size of the CO_2 perturbations. The uncertainty of the average differences plotted in Figs. 5 and 6 ranges between 1.2 and 2.3 %.

Another important issue is the spatial resolution of the retrieval products of the OXYCO2 experiment. The upper panels of Fig. 7 report, for the sample test, the vertical (left) and horizontal (right) resolutions of the retrieved CO_2 VMR field. They are calculated using the 2-D averaging kernel matrix as described in Carlotti et al. (2007). Since the correlation between CO_2 VMR and T is a major issue in our study, the same quantities as in the upper panels are reported in the lower panels of Fig. 7 for the retrieved T field. It can be seen in Fig. 7 that the vertical resolution of the retrieved CO_2 field is consistent with the geometrical sampling of the atmosphere (3 km) between 20 and 50 km. The horizontal resolution mostly exceeds the geometrical sampling of the retrieval grid with values lower than 350 km in the 20–50 km altitude range (to be compared with the 220 km of the retrieval grid). The complex interdependence between the many variables of the MTR inversion makes it difficult to interpret the 2-D distributions in the maps of Fig. 7. However, by looking at the IL maps of Fig. 2 and at the maps of Fig. 7, we can identify some correlation between the distributions of information load and those of spatial resolution. Finally, we remark that, since clouds represent an unquantified source of error, the results of our tests are only valid for cloud-free conditions.

4.4 Error budget

In this subsection we provide an estimate of the systematic error components that are associated with the choices implemented in the OXYCO2 experiment. As stated in Sect. 2.2, the MWs selection algorithm provides an estimate of the total error budget together with the contribution of the individual sources. This budget indicates that, among the considered error sources (see Sect. 2.2), the dominant components of the systematic error are the uncertainties on the VMRs of O_3,

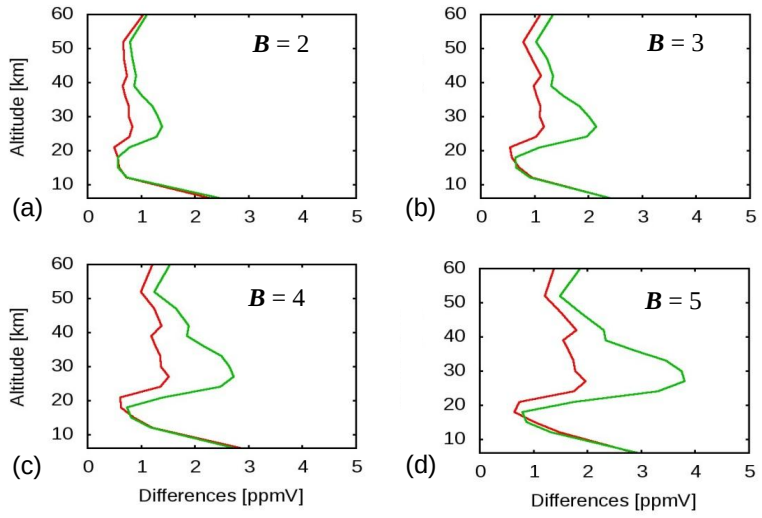

Figure 5. Red lines: overall plots for CO_2 retrievals in the case of B =2 for P- and B =1 for T-perturbations in Eq. (1); each panel contains the B value used for the CO_2 VMR perturbations. Green lines: same as red lines but excluding FIR MWs and H_2O parameters from the retrieval set-up.

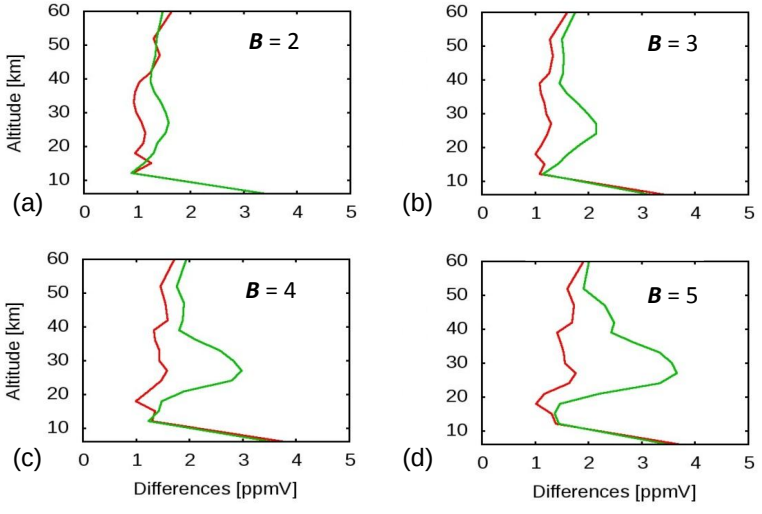

Figure 6. As Fig. 5 but in the case of $B = 3$ for the P- and $B = 4$ for the T-perturbations.

N_2O, and HNO_3, and the approximation introduced by the NLTE which is not modelled by the retrieval system. Since the 1-D retrieval algorithm used for the MWs selection differs in several aspects from GMTR, we have estimated the systematic errors introduced by the interfering species by repeating the sample test with the VMR profiles of O_3, N_2O, and HNO_3 perturbed according to their climatological variability. In the case of NLTE, the sample test was carried out on observations simulated by using the vibrational temperature profiles of the target species along the full orbit (that is irrespective of day–night conditions). We remark that, since we do not impose hydrostatic equilibrium in our retrievals, a possible constant pointing bias (due to the use of 1-D array detector; see Sect. 2.1) translates into the retrieval of an effective value of P at the vertical retrieval grid points. Therefore, if the resulting CO_2 VMR values are represented as a function of P, any bias in the pointing will be corrected. On the other hand, the errors on P have a negligible impact on the possibility of measuring the CO_2 VMRs (see Sect. 4.1). About the errors induced by the uncertainty of spectroscopic parameters (in particular those of CO_2 and O_2) we note that, if such an experiment will be considered for operational implementation, there will be dedicated measurements of them.

Figure 8 reports the main components and the total systematic error associated with the full set of 15 MWs used in our retrieval tests. The red curves of Figs. 5 and 6 compared to the total systematic error of Fig. 8 show that, below 50 km, the contribution of the systematic component of

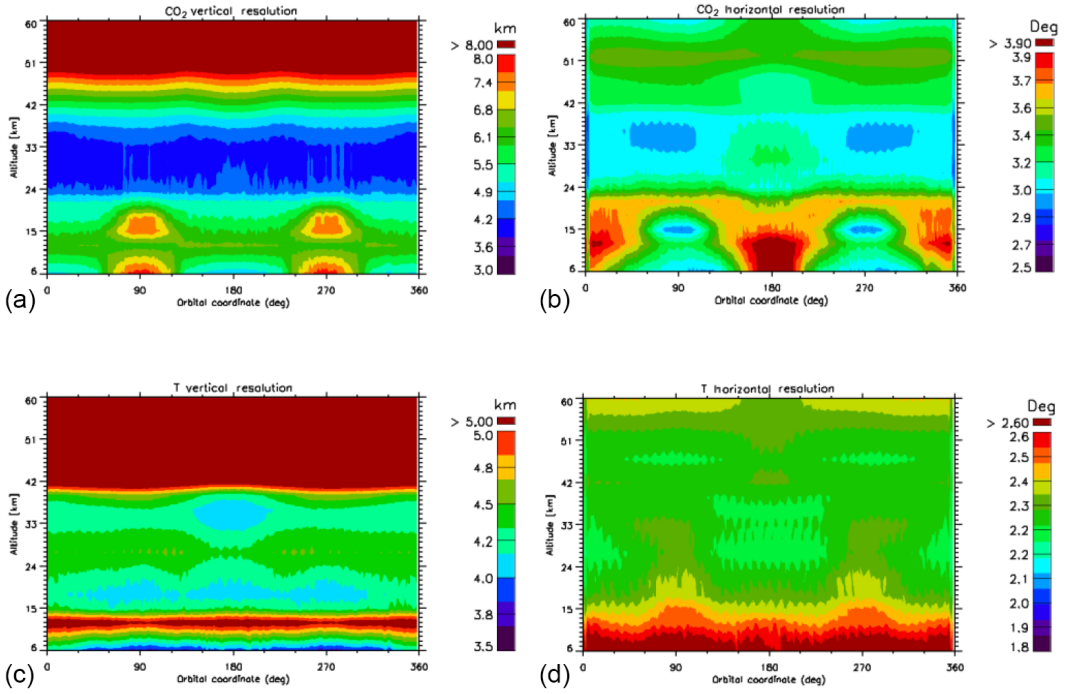

Figure 7. Maps of the vertical (**a** and **c**) and horizontal (**b** and **d**) resolutions as a function of altitude and orbital coordinate obtained with the averaging kernel matrix of the sample test retrieval. Panels **(a–b)** refer to the retrieved CO_2 field and panels **(c–d)** refer to the retrieved T field.

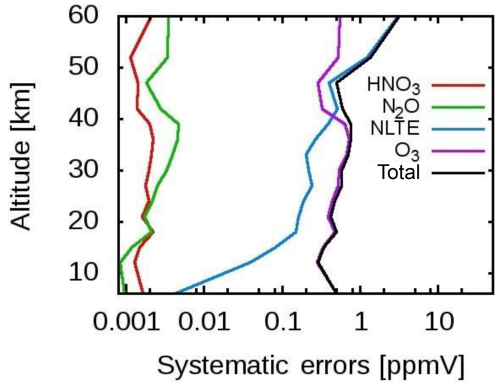

Figure 8. Error components and total systematic error associated with the set of 15 MWs that were used in retrieval tests. Only the three atmospheric gases that represent the main sources of error are reported. NLTE indicates the error propagated by neglecting non-local thermal equilibrium conditions in the retrieval system.

the total error is negligible with respect to the random component. However, the interference of the O_3 transitions turns out to be the most important source of systematic error below 40 km. This outcome justifies the relatively high spectral resolution adopted for OXYCO2 (see Sect. 2.1). Figure 8 also shows that above 50 km the capability of modelling NLTE is a limiting condition for the retrieval accuracy.

5 Conclusions

In this paper we have studied the possibility of measuring the CO_2 distributions in the stratosphere by exploiting the synergism between FIR and TIR limb-sounding measurements from space. The pure rotational transitions of O_2 in the FIR region are exploited to circumvent the strong correlation between T and CO_2 VMR, which is intrinsic in the analysis of CO_2 spectral features in the TIR region. In order to assess the performance of this concept, we have considered a hypothetical experiment (OXYCO2) based on a FT spectrometer for which we have defined instrumental and observational parameters. The proposed experiment is inspired by both previous experiments and previous studies for space limb sounders. The ability to measure CO_2 distributions was established through retrievals of OXYCO2 observations simulated at optimal spectral intervals.

We have shown that accurate T fields are necessary to retrieve CO_2 VMRs from the rovibrational spectra of this molecule with precisions of the order of 1 ppmv. For the analysis of FIR observations, the VMR of H_2O must be included in the state vector in order to avoid the systematic errors due to the interference of its spectral features. The best performance of the simulated retrievals is obtained when FIR and TIR observations are simultaneously analysed to derive CO_2 fields together with P, T, and H_2O fields.

A number of retrieval tests were carried out with the 2-D GMTR algorithm starting from initial guess profiles of the retrieval targets, obtained with different perturbations of the reference profiles. The outcome of these tests shows that a precision of the order of 1 ppmv can be achieved for the CO_2 VMRs in the altitude range between 10 and 50 km. These results have been obtained along a full orbit onto a vertical grid defined in steps of 3 km up to 42 km and 5 km above and onto a horizontal grid of profiles separated by about 220 km. The vertical resolution of the retrieved CO_2 fields is consistent with the retrieval grid between 20 and 50 km. The horizontal resolution depends on altitude and latitude and mostly exceeds the size of the retrieval grid; the best performance is in the 20–50 km altitude range where the horizontal resolution does not exceed 350 km.

If the FIR observations are excluded from the retrieval process, the precision of the CO_2 fields worsen by a factor which depends on altitude but may exceed 2 in the 20–40 km altitude range. This outcome demonstrates the starting hypothesis that FIR observations contribute to the CO_2 retrieval by introducing the information on T contained in the pure rotational spectrum of O_2.

The assessment of the systematic errors considered in this study (VMR of the atmospheric constituents and NLTE conditions) shows that below 50 km their contribution to the total error is negligible with respect to the random component. However, below 40 km the interference of O_3 transitions tends to be a meaningful source of systematic errors; therefore the spectral resolution needs to be high enough to ensure the retrieval accuracy to be driven by the random component of the error. Above 50 km, the accuracy of the CO_2 fields mainly depends on the capability of the retrieval system to model NLTE conditions.

Finally, we remark that the target of this study was the retrieval of CO_2 VMR fields. However, a number of side products can be identified within the spectral ranges of the OXYCO2 experiment, first of all the hydroxyl radical (OH, of fundamental importance in atmospheric chemistry), which displays unique spectral features around 118 cm^{-1} (Carlotti et al., 2001b). For the analysis of these features, FIR spectroscopy was identified as the best measurement strategy (PIRAMHYD, 1998).

6 Data availability

Data used in this study are available from the authors upon request.

Appendix A: The GMTR analysis system

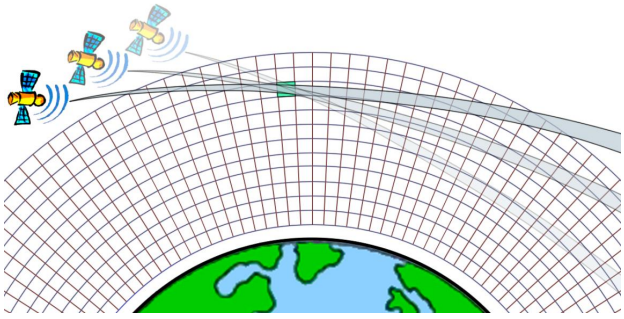

Figure A1. Picture illustrating the 2-D discretisation of the atmosphere and the merging of information from different observation geometries in the geo-fit analysis.

The GMTR analysis system (Carlotti et al., 2006) was developed as an open source code specifically designed for MIPAS measurements. It is based on the geo-fit approach (Carlotti et al., 2001a) upgraded with the multi-target retrieval (MTR) functionality (Dinelli et al., 2004). With the geo-fit, all the observations collected along the orbit track are analysed simultaneously by exploiting the continuous repetition of the limb sequences along the orbit plane. This repetition allows the gathering of information about a given parcel of atmosphere from all of the observations with a line of sight that crosses that parcel whatever limb sequence they belong to. This concept is illustrated in Fig. A1. Since the loop of overlap between nearby sequences closes when the atmospheric parcel sounded by the first sequence (preferably at North or South Pole) is observed again at the end of the orbit, the full gathering of information is achieved by merging the observations of the complete orbit into a simultaneous analysis. In the geo-fit the discretisation of the atmosphere is operated on both the vertical and the horizontal dimensions (Carlotti et al., 2001). In the vertical dimension altitude levels delimit atmospheric layers as in a 1-D approach. The horizontal discretisation is built using segments (called "radii") perpendicular to the Earth's geoid and extended up to the boundary of the atmosphere. The 2-D discretisation leads to a web-like picture in which consecutive levels and radii define plane figures called "cloves" while the points defined by the crossing of levels and radii are called "nodes" (Fig. A1 depicts the result). The value assumed by physical and chemical atmospheric quantities is assigned to each node by interpolating the profiles of the adopted atmospheric model. Therefore, the 2-D discretisation enables the modelling of horizontal atmospheric structures. The retrieval grid of the geo-fit is independent of the measurement grid so that atmospheric profiles can be retrieved with horizontal separations different from those of the measured limb scans. This strategy makes it possible to select the optimal horizontal resolution of the retrieved profiles on the basis of its trade-off with the precision of the retrieval parameters (Carlotti et al., 2007).

In the GMTR algorithm the observations are analysed with a constrained non-linear least-squares fit based on the Gauss–Newton method (Ridolfi et al., 2000; Carlotti et al., 2006; Carlotti et al., 2007). The iterative solution expression of this method is given by the following:

$$\boldsymbol{x}_{\mathrm{i}+1} = \boldsymbol{x}_{\mathrm{i}} + \left(\mathbf{K}_{\mathrm{i}}^{T}\mathbf{S}_{n}^{-1}\mathbf{K}_{i} + \mathbf{S}_{\mathrm{a}}^{-1}\right)^{-1} \left[\mathbf{K}_{i}^{T}\mathbf{S}_{n}^{-1}\boldsymbol{n}_{i} - \mathbf{S}_{\mathrm{a}}^{-1}\left(\boldsymbol{x}_{\mathrm{i}} - \boldsymbol{x}_{\mathrm{a}}\right)\right], \quad \text{(A1)}$$

where

- i denotes the iteration index,
- $\boldsymbol{x}_{\mathrm{i}}$ is the state vector at iteration i,
- $\boldsymbol{x}_{\mathrm{a}}$ is the vector containing the a priori state vector,
- $\boldsymbol{n}_i$ is the vector containing the differences between each observation and its value simulated by the forward model,
- $\mathbf{S}_n$ is the VCM of the vector $\boldsymbol{n}$,
- $\mathbf{K}_i$ is the matrix (Jacobian matrix) with rows containing the derivatives of each observation with respect to all of the retrieved parameters,
- $\mathbf{S}_{\mathrm{a}}$ is the variance–covariance matrix of the a priori state vector.

At the last iteration the errors associated with the solution of the inversion procedure are characterised by the VCM of $\boldsymbol{x}$ given by the following:

$$\mathbf{V}_x = \left(\mathbf{K}^{T}\mathbf{S}_{n}^{-1}\mathbf{K} + \mathbf{S}_{\mathrm{a}}^{-1}\right)^{-1} \quad \text{(A2)}$$

Matrix $\mathbf{V}_x$ maps the measurement random errors (represented by $\mathbf{S}_n$) onto the uncertainty of the values of the retrieved parameters; in particular, the square root of the diagonal element p of $\mathbf{V}_x$ provides the estimated standard deviation (ESD) of the corresponding parameter:

$$\mathrm{ESD}_{\mathrm{p}} = \left[\left(\mathbf{V}_x\right)_{\mathrm{p,p}}\right]^{1/2}. \quad \text{(A3)}$$

The information load analysis

In the 2-D approach it is possible to associate a quantifier to each clove of the atmospheric discretisation, which measures the amount of information carried by that clove with respect to a retrieval target (Carlotti and Magnani, 2009). The information load quantifier (Ω) of clove h with respect to atmospheric parameter q is defined as follows (Carlotti and Magnani, 2009):

$$\Omega\left(q,h\right) = \left[\sum_{i=1}^{l}\sum_{j=1}^{m}\sum_{k=1}^{n}\left(\frac{\partial Y_{ijk}}{\partial q_h}\right)^{2}\right]^{1/2}, \quad \text{(A4)}$$

where

- Y_{ijk} is the spectral radiance of observation geometry i at wave number k of the analysed MW j,
- l is the number of observation geometries that crosses the clove h,
- m is the number of spectral intervals analysed in observation geometry i,
- n is the number of spectral points in spectral interval j.

In Eq. (A4) the triple summation could be grouped in a single summation over all of the spectral radiances that are affected by the value of q in clove h. Therefore, the column vector containing the whole set of elements within the triple summation of Eq. (A4) is the Jacobian matrix corresponding to the retrieval of the scalar value of q in clove h, and (moving to the lower-case notation for $\mathbf{K}$ that represents now a vector) we can write Eq. (A4) as follows:

$$\Omega = \left(\boldsymbol{k}^T \boldsymbol{k}\right)^{1/2}. \tag{A5}$$

On the other hand, if we assume an unconstrained retrieval on observations that are uncorrelated and characterised by constant uncertainty $\mathbf{S}_n = \mathbf{I}$, Eq. (A2) becomes

$$\mathbf{V}_q = \left(\boldsymbol{k}^T \boldsymbol{k}\right)^{-1}. \tag{A6}$$

Hence, it follows from Eq. (A3) that the ESD of the retrieved value of q in clove h is given by $1/\Omega$. These considerations justify the quadratic summation as combination rule of the partial derivatives in Eq. (A4). Further on, if the observations are correlated and characterised by the VCM $\mathbf{S}_n$, Ω can be calculated as

$$\Omega = \left(\boldsymbol{k}^T \mathbf{S}_n \boldsymbol{k}\right)^{1/2}. \tag{A7}$$

The values of the information load can be calculated for each clove of the 2-D discretisation so that we can draw, for each retrieval target, a map of the 2-D distribution of the Ω quantifier. The information load maps provide a picture of the "real" atmospheric sampling of the observations. They can be used to define optimal retrieval grids (where the information peaks) or to compare the atmospheric sampling for different targets or for different observation strategies. The information load analysis is, therefore, suitable for studying the performance of different experimental conditions.

Acknowledgements. The MWs selection task was carried out by exploiting an Erasmus+ Traineeship 2014/2015 grant at Oxford University, with the supervision of Anu Dudhia, whom we thank for his valuable contribution.

Edited by: H. Worden
Reviewed by: C. Sioris and one anonymous referee

References

Bernath, P. F., McElroy, C. T., Abrams, M. C., Boone, C. D., Butler, M., Camy-Peyret, C., Carleer, M., Clerbaux, C., Coheur, P.-F., Colin, R., DeCola, P., DeMaziere, M., Drummond, J. R., Dufour, D., Evans,W. F. J., Fast, H., Fussen, D., Gilbert, K., Jennings, D. E., Llewellyn, E. J., Lowe, R. P., Mahieu, E., McConnel, J. C., McHugh, M., Mcleod, S. D., Michaud, R., Midwinter, C., Nassar, R., Nichitiu, F., Nowland, C., Rinsland, C. P., Rochon, Y. J., Rowlands, N., Semeniuk, K., Simon, P., Skelton, R., Sloan, J. J., Soucy, M. A., Strong, K., Tremblay, P., Turnbull, D., Walker, K. A., Walkty, I., Wardle, D. A., Wehrle, V., Zander, R., and Zou, J.: Atmospheric Chemistry Experiment (ACE): Misson overview, Geophys. Res. Lett., 32, L15S01, doi:10.1029/2005GL022386, 2005.

Bianchini, G., Cortesi, U., Palchetti, L., and Pascale, E.: SAFIRE-A (spectroscopy of the atmosphere by far-infrared emission-airborne): optimized instrument configuration and new assessment of improved performance, Appl. Optics, 43, 2962–2977, doi:10.1364/AO.43.002962, 2004.

Boesch, H., Baker, D., Connor, B., Crisp, D., and Miller, C.: Global characterization of CO_2 column retrievals from shortwave-infrared satellite observations of the orbiting carbon observatory-2 mission, Remote Sens., 3, 270–304, doi:10.3390/rs3020270, 2011.

Buchwitz, M., de Beek, R., Noël, S., Burrows, J. P., Bovensmann, H., Bremer, H., Bergamaschi, P., Körner, S., and Heimann, M.: Carbon monoxide, methane and carbon dioxide columns retrieved from SCIAMACHY by WFM-DOAS: year 2003 initial data set, Atmos. Chem. Phys., 5, 3313–3329, doi:10.5194/acp-5-3313-2005, 2005.

Carli, B. and Carlotti, M.: Far-Infrared and Microwave Spectroscopy of the Earth's Atmosphere, in: Spectroscopy of the Earth's Atmosphere and Interstellar Medium, edited by: Rao, K. N. and Weber, A., Academic Press, Boston, USA, 1–95, doi:10.1016/B978-0-12-580645-9.50005-8, 1992.

Carlotti, M. and Magnani, L.: Two-dimensional sensitivity analysis of MIPAS observations, Opt. Express 17, 5340–5357, doi:10.1364/OE.17.005340, 2009.

Carlotti, M., Dinelli, B. M., Raspollini, P., and Ridolfi, M.: Geo-fit approach to the analysis of limb-scanning satellite measurements, Appl. Optics, 40, 1872–1885, doi:10.1364/AO.40.001872, 2001a.

Carlotti, M., Ade, P. A. R., Carli, B., Chipperfield, M., Hamilton, P. A., Mencaraglia, F., Nolt, I. G., and Ridolfi, M.: Diurnal variability and night detection of stratospheric hydroxyl radical from far infrared emission measurements, JASTP, 63/14, 1509–1518, doi:10.1016/S1364-6826(01)00030-X, 2001b.

Carlotti, M., Brizzi, G., Papandrea, E., Prevedelli, M., Ridolfi, M., Dinelli, B. M., and Magnani, L.: GMTR: Two-dimensional multi-target retrieval model for Michelson Interferometer for Passive Atmospheric Sounding/Environmental Satellite observations, Appl. Optics, 45, 716–727, doi:10.1364/AO.45.000716, 2006.

Carlotti, M., Dinelli, B. M., Papandrea, E., and Ridolfi, M.: Assessment of the horizontal resolution of retrieval products derived from MIPAS observations, Opt. Express, 15, 10458–10472, doi:10.1364/OE.15.010458, 2007.

Carlotti, M., Arnone, E., Castelli, E., Dinelli, B. M., and Papandrea, E.: Position error in profiles retrieved from MIPAS observations with a 1-D algorithm, Atmos. Meas. Tech., 6, 419–429, doi:10.5194/amt-6-419-2013, 2013.

Chédin, A., Scott, N. A., Crevoisier, C., and Armante, R.: First global measurement of midtropospheric CO_2 from NOAA polar satellites: the tropical zone, J. Geophys. Res., 108, 4581, doi:10.1029/2003JD003439, 2003.

Crevoisier, C., Heilliette, S., Chédin, A., Serrar, S., Armante, R., and Scott, N. A.: Midtropospheric CO_2 concentration retrieval from AIRS observations in the tropics, Geophys. Res. Lett., 31, L17106, doi:10.1029/2004GL020141, 2004.

Crevoisier, C., Chédin, A., Matsueda, H., Machida, T., Armante, R., and Scott, N. A.: First year of upper tropospheric integrated content of CO_2 from IASI hyperspectral infrared observations, Atmos. Chem. Phys., 9, 4797–4810, doi:10.5194/acp-9-4797-2009, 2009.

Dinelli, B. M., Alpaslan, D., Carlotti, M., Magnani, L., and Ridolfi, M.: Multi–target retrieval (MTR): the simultaneous retrieval of pressure, temperature and volume mixing ratio profiles from limb–scanning atmospheric measurements, J. Quant. Spectrosc. Ra., 84, 141–157, doi:10.1016/S0022-4073(03)00137-7, 2004.

Dudhia, A., Jay, V. L., and Rodgers, C.: Microwindow selection for high-spectral-resolution sounders, Appl. Optics, 41, 3665–3673, doi:10.1364/AO.41.003665, 2002.

Emmert, J. T., Stevens, M. H., Bernath P. F., Drob, D. P., and Boone, C. D.: Observations of increasing carbon dioxide concentration in Earth's thermosphere, Nat. Geosci., 5, 868–871, 2012.

Fischer, H., Birk, M., Blom, C., Carli, B., Carlotti, M., von Clarmann, T., Delbouille, L., Dudhia, A., Ehhalt, D., Endemann, M., Flaud, J. M., Gessner, R., Kleinert, A., Koopman, R., Langen, J., López-Puertas, M., Mosner, P., Nett, H., Oelhaf, H., Perron, G., Remedios, J., Ridolfi, M., Stiller, G., and Zander, R.: MIPAS: an instrument for atmospheric and climate research, Atmos. Chem. Phys., 8, 2151–2188, doi:10.5194/acp-8-2151-2008, 2008.

Foucher, P. Y., Chédin, A., Dufour, G., Capelle, V., Boone, C. D., and Bernath, P.: Technical Note: Feasibility of CO_2 profile retrieval from limb viewing solar occultation made by the ACE-FTS instrument, Atmos. Chem. Phys., 9, 2873–2890, doi:10.5194/acp-9-2873-2009, 2009.

Foucher, P. Y., Chédin, A., Armante, R., Boone, C., Crevoisier, C., and Bernath, P.: Carbon dioxide atmospheric vertical profiles retrieved from space observation using ACE-FTS solar occultation instrument, Atmos. Chem. Phys., 11, 2455–2470, doi:10.5194/acp-11-2455-2011, 2011.

Gille, J., Barnett, J., Arter, P., Barker, M., Bernath, P., Boone, C., Cavanaugh, C., Chow, J., Coffey, M., Craft, J., Craig, C., Dials, M., Dean, V., Eden, T., Edwards, D. P., Francis, G., Halvorson, C., Harvey, L., Hepplewhite, C., Khosravi, R., Kinnison, D., Krinsky, C., Lambert, A., Lee, H., Lyjak, L., Loh, J., Mankin, W., Massie, S., McInerney, J., Moorhouse, J., Nardi, B., Pack-

man, D., Randall, C., Reburn, J., Rudolf, W., Schwartz, M., Serafin, J., Stone, K., Torpy, B., Walker, K., Waterfall, A., Watkins, R., Whitney, J., Woodard, D., and Young, G.: High Resolution Dynamics Limb Sounder: experiment overview, recovery and validation of initial temperature data, J. Geophys. Res., 113, D16S43, doi:10.1029/2007JD008824, 2008.

Kraft, S., Caron, J., Bézy, J. L., Meynart, R., Langen, J., Dominguez, B. C., Bensi, P., and Silvestrin, P.: PREMIER's Imaging IR Limb Sounder, Proc. SPIE 8176, 10, doi:10.1117/12.898328, 2011.

Kulawik, S. S., Jones, D. B. A., Nassar, R., Irion, F. W., Worden, J. R., Bowman, K. W., Machida, T., Matsueda, H., Sawa, Y., Biraud, S. C., Fischer, M. L., and Jacobson, A. R.: Characterization of Tropospheric Emission Spectrometer (TES) CO_2 for carbon cycle science, Atmos. Chem. Phys., 10, 5601–5623, doi:10.5194/acp-10-5601-2010, 2010.

Kuze, A., Suto, H., Nakajima, M., and Hamazaki, T.: Initial Onboard Performance of TANSO-FTS on GOSAT, in Fourier Transform Spectroscopy, OSA Technical Digest, OSA Proc., doi:10.1364/FTS.2009.FTuC2, 2009.

Lim, T. L., Burgdorf, M. J., Swinyard, B. M., Tommasi, E., Griffin, M. J., and Clegg, P. E.: Long-term performance of doped Ge:Ga photoconductors in the space environment, Proc. SPIE 3354, Infrared Astronomical Instrumentation, 347, doi:10.1117/12.317321, 1998.

PIRAMHYD Retrieval Study: OH Profiling by Far Infrared Limb Sounding, Final Report, ESA CR(P), 4195, by: SERCO, SRON, IROE-CNR, RAL. DLR, 1998.

Remedios, J. J., Leigh, R. J., Waterfall, A. M., Moore, D. P., Sembhi, H., Parkes, I., Greenhough, J., Chipperfield, M. P., and Hauglustaine, D.: MIPAS reference atmospheres and comparisons to V4.61/V4.62 MIPAS level 2 geophysical data sets, Atmos. Chem. Phys. Discuss., 7, 9973–10017, doi:10.5194/acpd-7-9973-2007, 2007.

Ridolfi, M., Carli, B., Carlotti, M., von Clarmann, T., Dinelli, B. M., Dudhia, A., Flaud, J. M., Hoepfner, M., Morris, P. E., Raspollini, P., Stiller, G., and Wells, R. J.: Optimized forward model and retrieval scheme for MIPAS near-real-time data processing, Appl. Optics, 39, 1323–1340, doi:10.1364/AO.39.001323, 2000.

Rogalski, A.: Progress in focal plane array technologies, Progress in Quantum Electronics, 36, March–May 2012, 342–473, ISSN 0079-6727, doi:10.1016/j.pquantelec.2012.07.001, 2012.

Sioris, C. E., Boone, C. D., Nassar, R., Sutton, K. J., Gordon, I. E., Walker, K. A., and Bernath, P. F.: Retrieval of carbon dioxide vertical profiles from solar occultation observations and associated error budgets for ACE-FTS and CASS-FTS, Atmos. Meas. Tech., 7, 2243–2262, doi:10.5194/amt-7-2243-2014, 2014